ACS Catalysis

Research Article

pubs.acs.org/acscatalysis

Terms of Use

Exploring the Origin of Enhanced Activity and Reaction Pathway for Photocatalytic H_2 Production on Au/B-TiO_2 Catalysts

Fenglong Wang,[†] Yijiao Jiang,*[,†] Anil Gautam,[‡] Yarong Li,[‡] and Rose Amal*[,†]

[†]School of Chemical Engineering, The University of New South Wales, Sydney, New South Wales 2052, Australia

[‡]Environmental Protection Science Branch, Office of Environment and Heritage, Lidcombe, New South Wales 1825, Australia

Supporting Information

ABSTRACT: Gold-embedded boron-doped TiO_2 (Au/B-TiO_2) photocatalysts were synthesized by a sol−gel hydrothermal method. The TEM images display that the gold nanoparticles were embedded into the B-TiO_2 framework. Hydrogen evolution under light irradiation showed that doping of boron into TiO_2 enhanced the photocatalytic activity. A further remarkable improvement of the activity was observed over the Au/B-TiO_2. Evidenced by B 1s XPS and ^{11}B MAS NMR spectra, the embedment of Au nanoparticles contributes to the formation of more interstitial boron species in B-TiO_2. In turn, it gives rise to surface or near-surface states facilitating the embedment of Au nanoparticles, as demonstrated by the Au 4f XPS spectra, which indicates the strong interaction between gold and the B-TiO_2 framework. This specific synergy significantly contributes to the enhancement of photocatalytic activity. For the first time, the isotopic tracer studies using a gas chromatograph isotope ratio mass spectrometer along with a series of control experiments reveal that the produced hydrogen originated mainly from water rather than methanol, whereas the direct oxidation of methanol did not lead to hydrogen generation. Acting as a sacrificial reagent, methanol could be oxidized to formaldehyde by protons/water under oxygen-free conditions.

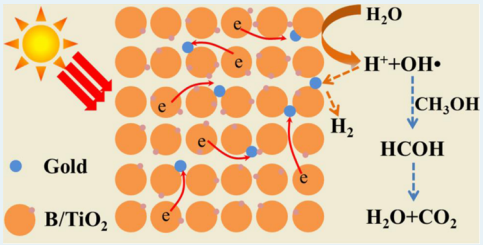

KEYWORDS: *embedded gold, doped boron, hydrogen production, isotope tracer, reaction pathway*

INTRODUCTION

With the global depletion of fossil-based energy resources, solar fuels technology has been considered to be a promising route to generate alternative and renewable energy carriers, in particular, hydrogen.[1] Heterogeneously photocatalytic systems based on titanium dioxide (TiO_2) have been studied primarily for environmental remediation[2] and eventually expanded in hydrogen production from water.[3] In TiO_2-based photocatalysis, the electrons and holes are generated by photoexcitation, and subsequently, the photogenerated charge carriers are migrated to the surface and initiate the redox reaction. Two excited electrons in the conduction band are required to reduce aqueous protons to one hydrogen molecule, whereas the photoinduced holes are generally trapped by sacrificial reagents, such as alcohols or organic acids. In this system, an oxygen-free condition is highly desirable because oxygen molecules preferentially scavenge the photoinduced electrons to suppress hydrogen generation.[4]

Because of the fast recombination rate between the photoinduced charge carriers and the anoxic condition in photocatalytic hydrogen production, it is imperative to tailor TiO_2 materials in a suitable manner to enhance hydrogen evolution.[5] One promising approach to improve the photocatalytic activity of TiO_2 is to modify the surface with noble metal nanoparticles to enhance the charge separation.[6] It has been well documented that with the presence of a metal with a larger work function, that is, lower Fermi level, the photoinduced electrons can be easily trapped, which results in boosting the photocatalytic efficiency.[7] Instead of depositing gold nanoparticles on the surface of TiO_2, Lu et al. inserted gold nanoparticles into the TiO_2 framework to prevent Au particle from agglomeration and leaching in an aqueous system, leading to superior activity and long durability in organic degradation and chromium reduction.[8]

Anion doping, such as N, C, S, F, and B, has been shown to enhance the photocatalytic performance of TiO_2.[9] Unlike N-doping, the number of studies demonstrating the effectiveness of boron doping remains very limited. Lambert et al. studied the B-doped and B,N-codoped TiO_2 photocatalysts for the degradation of methyl tertiary butyl ether.[10] Both boric oxide-like and doped species in the lattice of TiO_2 were identified, and the later induced visible light absorption. Liu et al. reported the TiO_2 doped with 10 at. % B showed the highest visible light activity for degradation of Rhodamine B.[11] By ^{11}B solid-state NMR spectroscopy combined with density functional theory calculations, Deng's group have identified several boron sites in the B-doped and B,N-codoped TiO_2.[12] Recently, they have presented evidence that the origin of the high activity of Ag,B-codoped TiO_2 photocatalysts in methylene blue degradation lies on the formation of interstitial boron species, which tend to lead to a decrease in the band gap.[13]

Received: March 5, 2014
Revised: March 31, 2014
Published: March 31, 2014

   dx.doi.org/10.1021/cs5002948 | ACS Catal. 2014, 4, 1451−1457

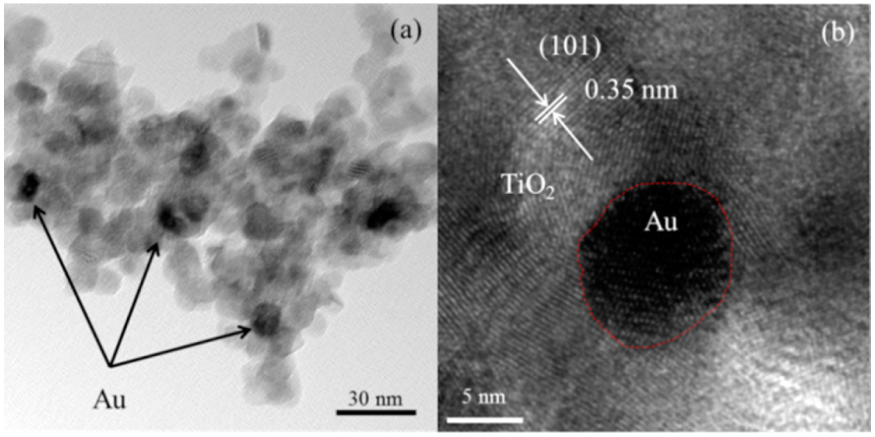

Figure 1. TEM images of $Au_{0.5}/B\text{-}TiO_2$ with (a) low and (b) high magnification.

Surface modification with both anions (F or P) and metals on the surface of TiO_2 has been recently reported for simultaneous hydrogen generation with the degradation of organic pollutants.[4,14] Because anion-doped TiO_2 does not suffer from thermal instability, a robust synthetic method needs to be developed. In this work, novel Au-embedded, B-doped TiO_2 ($Au/B\text{-}TiO_2$) photocatalysts were synthesized by a one-pot sol–gel hydrothermal method and tailored for photocatalytic hydrogen generation from a water/methanol mixture. The $Au/B\text{-}TiO_2$ exhibits great enhancement in hydrogen evolution compared with the solely B-doped TiO_2 and Au-embedded TiO_2. Furthermore, our mechanistic studies in this work have first answered the most important question during this process: *Where does the hydrogen come from?* Gas chromatograph/isotope ratio mass spectrometer (GC/IRMS) is a highly specialized technique employed in this study to ascertain the relative ratio of hydrogen ($^2H/^1H$) in hydrogen, water, and methanol molecules. For the first time, the isotopic tracer studies based on GC/IRMS indicates that the evolved hydrogen originated mainly from water rather than methanol.

EXPERIMENTAL SECTION

$Au/B\text{-}TiO_2$ catalysts were synthesized through a one-pot sol–gel hydrothermal method. In a typical process, a given amount of boron acid (molar ratio of B/Ti is 10%) and gold(III) chloride trihydrate (molar ratio of Au/Ti is 0, 0.1%, 0.5%, 1%, and 2%) were dissolved in 70 mL of ethanol–water mixture to form a uniform solution, then 5 mL of titanium tetraisopropoxide was injected into the system under vigorous stirring. The obtained suspension was aged for 15 h and then transferred into a 100 mL Teflon-lined autoclave for hydrothermal treatment at 140 °C for 12 h. Afterward, the products were centrifuged and washed with ethanol and water and then dried at 60 °C. The as-synthesized powder was calcined at 400 °C for 4 h. The bare TiO_2 and Au/TiO_2 without boron doping were synthesized using the same method. The obtained products are denoted as TiO_2, $B\text{-}TiO_2$, $Au_{0.5}/TiO_2$, $Au_{0.1}/B\text{-}TiO_2$, $Au_{0.5}/B\text{-}TiO_2$, $Au_1/B\text{-}TiO_2$, and $Au_2/B\text{-}TiO_2$, respectively.

Transmission electron microscopy (TEM) analysis was performed on a Phillips CM200 facility. UV–vis diffuse reflectance spectra (UV–vis) were obtained on a Shimadzu UV 3600 spectrophotometer. Raman spectra were obtained from a PerkinElmer Raman station 400 instrument using an exposure time of 1 s and an interval of 2 cm^{-1} for four scans. X-ray photoelectron spectroscopy (XPS) studies were conducted on an Escalab250Xi spectrometer (Thermo Scientific, UK) applying a monochromated Al Kα source at 15.2 kV and 168 W. The ^{11}B magic angle spinning nuclear magnetic resonance (MAS NMR) experiments were performed on a Bruker Avance III 300 spectrometer at a resonance frequency of 96 MHz. A 4 mm rotor and a spinning frequency of 12 kHz were used. The ^{11}B chemical shifts were referenced to that of $NaBH_4$.

The photocatalytic hydrogen production was performed on a top-irradiation reactor cell with a 300 W xenon arc lamp as light source. In a typical procedure, 50 mg of the catalysts was dispersed in 100 mL of water/methanol mixture (volume ratio = 9:1) under sonication. Argon was purged into the system for more than 30 min to completely vent out the air. The mixture was then irradiated under vigorous stirring, and a water jacket was placed on top of the reactor to absorb the heat. The evolved gas was analyzed every 30 min using gas chromatography (GC, 8A, Shimadzu) equipped with a thermal conductivity detector.

To explore the origin of hydrogen generated during the photocatalytic process, isotopic tracer experiments, that is, deuterium oxide (D_2O, Sigma-Aldrich, 99.9% D) or deuterated methanol (CD_3OD, Sigma-Aldrich, 99.8% D) was used under the identical conditions. A gas chromatograph (Thermo Trace GC Ultra) coupled with isotope ratio mass spectrometer (Thermo Delta V Plus) was used to monitor the gaseous components accumulated in the headspace of the suspension upon light irradiation. The gaseous samples containing hydrogen, water, and methanol were injected into the GC/IRMS system. First, hydrogen, water, and methanol were separated in the GC column (RT-U-BOND, 30 m × 0.32 mm × 10 μm), and then the separated components sequentially entered into a reactor, where they were converted into hydrogen, carbon monoxide, and carbon deposits. The isotopic composition of hydrogen (mass 2 for H–H and mass 3 for H–D) were monitored using an isotope ratio mass spectrometer. Three hydrogen peaks in the chromatograms are attributed to the photocatalytically evolved hydrogen, hydrogen in water, and hydrogen in methanol, respectively. The order of retention time was confirmed using single reference standards of hydrogen, water, and methanol. A high-performance liquid chromatograph (HPLC) using a Waters alliance 2695 module coupled with a Waters 410 differential refractometer was employed to detect the aqueous intermediates/products in the photocatalytic process.

dx.doi.org/10.1021/cs5002948 | ACS Catal. 2014, 4, 1451–1457

RESULTS AND DISCUSSION

Figure 1 shows the typical TEM images of the $Au_{0.5}/B\text{-}TiO_2$ sample under a low and high magnification. It is observed that the gold particles are well-dispersed and embedded into the TiO_2 framework. A dark Au particle with a size of ~8 nm is seen in Figure 1b. The XRD patterns in Supporting Information Figure S1 show that with an increase in the Au content, the intensity of the diffraction peaks of gold grows. The continuity of the TiO_2 lattice on the dark dot confirms that the gold particle was integrated into the TiO_2 matrix. Having embedded gold particles strongly interact with the TiO_2 framework would result in efficient electron transfer from the TiO_2 to gold particles.[8b] In addition, with gold introduced into the framework, the distance required for the electron transportation from TiO_2 to Au is shortened compared with the distance to the outer surface of the TiO_2, thus hindering the recombination and leading to enhanced activity.[15] In addition, previous research indicated that the encapsulation texture showed superior activity and long durability due to the less agglomeration and leaching of the gold nanoparticles during organic oxidation and chromium reduction in aqueous condition.[8]

Figure 2 displays the UV−vis absorption spectra of all the catalysts present in this work. After doping of boron, neither

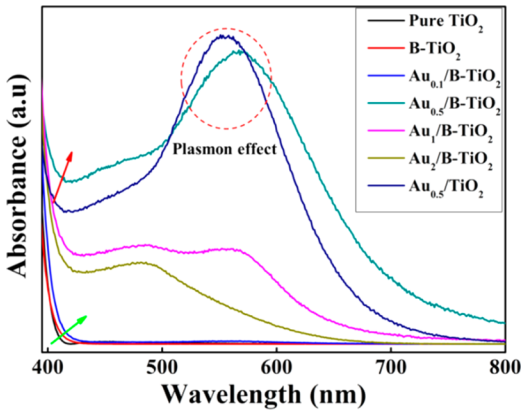

Figure 2. UV−vis absorption spectra of the pure TiO_2, B-TiO_2, $Au_{0.5}/TiO_2$, and $Au_x/B\text{-}TiO_2$ (x = 0.1, 0.5, 1, 2).

absorption edge shift nor appreciable enhancement of visible light absorption was observed on the B-TiO_2 compared with the bare TiO_2. With 0.1% of embedded Au, a slight enhancement of visible light absorption was observed. When the content of gold increased to 0.5% ($Au_{0.5}/B\text{-}TiO_2$ and $Au_{0.5}/TiO_2$), the absorption intensity in the visible region of ~500−600 nm was dramatically increased. The enhanced absorption can be attributed to the surface plasmon resonance effect.[16] Further increasing the content of gold up to 2%, however, led to a decrease in the plasmonic effect.[17] This might be attributed to the growth of the gold nanoparticles, which is confirmed by the XRD results.

The Raman spectra of the representative samples in the range from 100 to 700 cm^{-1} are shown in Figure 3. The peaks at 145, 395, 510, and 635 cm^{-1} can be assigned to the E_g, B_{1g}, A_{1g} modes of the anatase phase, respectively.[8b] The absorption became weaker after doping of boron and embedding of Au. It is evident that after the introduction of gold, both $Au_{0.5}/TiO_2$ and $Au_{0.5}/B\text{-}TiO_2$ show much weaker and broader Raman peaks at the position of 154 cm^{-1}, with a positive shift by 9

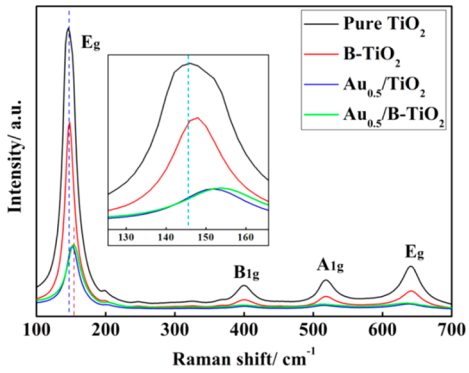

Figure 3. Raman spectra of the pure TiO_2, B-TiO_2, $Au_{0.5}/TiO_2$, and $Au_{0.5}/B\text{-}TiO_2$.

cm^{-1}. These shifts can be attributed to the increase in the crystalline defects within the nanocomposites as a result of the distortion caused by the embedded gold nanoparticles, and such defects may promote capturing of the photogenerated electrons, thus improving the photocatalytic activity.[8b] Moreover, the Au particles embedded into the nanocomposites can serve as the electron sinks and act as the reactive sites for the proton reduction in the suspension.

The hydrogen evolution was compared among the bare TiO_2, B-TiO_2, $Au_{0.5}/TiO_2$, and $Au_{0.5}/B\text{-}TiO_2$ in the presence of methanol as a sacrificial reagent, as shown in Figure 4. For all

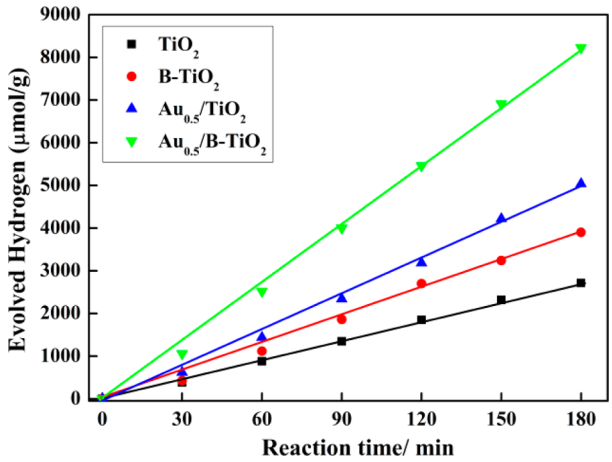

Figure 4. Hydrogen evolution from a water/methanol mixture (volume ratio = 9:1) in the suspension containing the bare TiO_2, B-TiO_2, $Au_{0.5}/TiO_2$, or $Au_{0.5}/B\text{-}TiO_2$ under light irradiation (Xe lamp, 300 W) for 3 h.

the photocatalysts, the evolution of hydrogen gas started upon light irradiation (Xe lamp, 300 W). The linear increase in the evolved hydrogen indicates the stability of the materials. The bare TiO_2 shows the lowest activity with the hydrogen evolution of 2700 μmol/g within 3 h. After doping with boron, the material of B-TiO_2 exhibits a better property with the hydrogen generation of 3900 μmol/g. When gold nanoparticles were embedded into the TiO_2 materials, the photocatalytic performance was further enhanced to 5040 μmol/g. When the Au/Ti molar ratio was kept at 0.5%, $Au_{0.5}/B\text{-}TiO_2$ could produce 8220 μmol/g of hydrogen within 3 h, much higher than that of $Au_{0.5}/TiO_2$. The results indicate that the doping of boron plays a positive role in increasing the hydrogen generation efficiency, and after introduction of gold,

dx.doi.org/10.1021/cs5002948 | ACS Catal. 2014, 4, 1451−1457

the enhancement was boosted as a result of the synergistic effect of the metal and anion coexistence.

To study the effect of the Au content on the activity of the Au-embedded B-TiO_2 materials, Figure 5 compares the

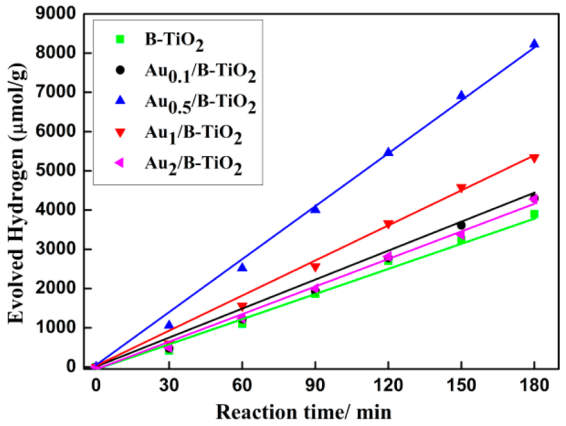

Figure 5. Hydrogen evolution from a water/methanol mixture (volume ratio = 9:1) in the suspension containing Au_x/B-TiO_2 (x = 0.1, 0.5, 1, 2) under light irradiation (Xe lamp, 300 W) for 3 h.

hydrogen generation efficiency using different Au contents. The hydrogen evolution continuously increased from 3900 to 4300 and further to 8220 μmol/g when the Au content was increased from 0 to 0.5%. Nearly twice the evolution of hydrogen gas was achieved when 0.5% of Au was embedded into the B-TiO_2 composite. An additional increase in the Au loading, however, led to a decrease in the activity. This finding shows 0.5% of gold is the optimal content. When the content is below this value, there are insufficient gold nanoparticles as the electron traps. When the Au content is too high, many of the gold nanoparticles would act as recombination centers for the excited charge carriers, resulting in lower activity.

The B 1s XPS peak of B-TiO_2 shown in Figure 6a was deconvoluted into two overlapped peaks centered at 191.6 and 192.1 eV, corresponding to the doped boron species (Ti−O−B) in the TiO_2 lattice and surface B_2O_3 species (with XPSPEAK 41software).[12,18] Similarly, two peaks centered at 191.6 and 192.6 eV were also obtained for the $Au_{0.5}$/B-TiO_2 (Figure 6b). It is well accepted that boron oxide has no response to light irradiation; however, it has been proposed that the presence of the Ti−O−B species could contribute to visible light absorption, leading to enhancement of organic pollutant photodegradation.[10,13,18,19] However, no apparent absorption in the visible region was seen in our UV−vis spectrum of the B-TiO_2 (Figure 2).

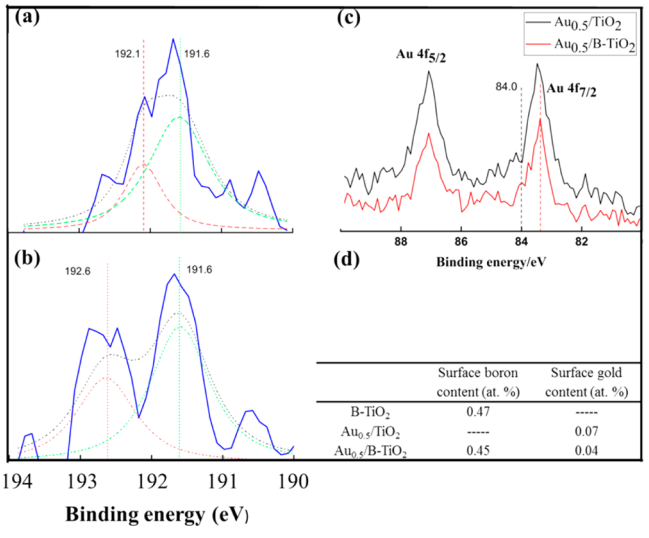

Figure 6. B 1s XPS spectra of the (a) B-TiO_2 and (b) $Au_{0.5}$/B-TiO_2, (c) Au 4f XPS spectra obtained from $Au_{0.5}$/TiO_2 and $Au_{0.5}$/B-TiO_2, and (d) the surface B and Au contents based on the XPS analysis for the above samples.

Deng's group has recently proposed that the presence of the interstitial boron species in anatase TiO_2 was prone to form defects, which could provide space for implanting Ag into the codoped TiO_2 lattice by substituting the Ti site, forming the substitutional Ag (B−O−Ag).[13] In this study, it appears that the formation of the Ti−O−B structure provides vacancies or microvoids for gold ions that were converted into gold metal after calcination. On the other hand, the incorporation of gold ions promotes the formation of the Ti−O−B structure, as discussed in the following NMR results. The increased content of such Ti−O−B structure resulted in the improvement of the activity. It could be explained that the embedded gold nanoparticles probably sitting in close proximity to these structures act as efficient sinks for the photoexcited electrons, which in turn prolongs the lifetime of the charge carriers and enhances the activity.

The oxidation states of gold in the $Au_{0.5}$/TiO_2 and $Au_{0.5}$/B-TiO_2 samples were studied by XPS spectroscopy. As shown in Figure 6c, gold species in both $Au_{0.5}$/TiO_2 and $Au_{0.5}$/B-TiO_2 are present in the metallic state, as indicated by Au $4f_{7/2}$ peaks at 83.4 eV. Compared with the Au $4f_{7/2}$ peaks obtained from the bulk gold materials (84.0 eV), the peaks observed are negatively shifted toward a lower binding energy region of 83.4 eV, indicating the strong interaction between gold particles and TiO_2 framework and efficient electron transfer from the conduction band of TiO_2 to the gold particles.[8b,20] From the surface element content analysis (Figure 6d), the surface Au contents of both the $Au_{0.5}$/TiO_2 and $Au_{0.5}$/B-TiO_2 samples are quite low (<0.1 at. %), indicating that most of the gold might be embedded into the framework of TiO_2 materials. Therefore, the interaction between gold and TiO_2 can be stronger. In addition, embedding the Au particles into the TiO_2 framework protects the Au particles from leaching.[8a]

^{11}B MAS NMR is a powerful technique for characterizing the chemical environment of B-species.[21] ^{11}B MAS NMR spectra of the B-TiO_2 and $Au_{0.5}$/B-TiO_2 samples are shown in Figure 7.

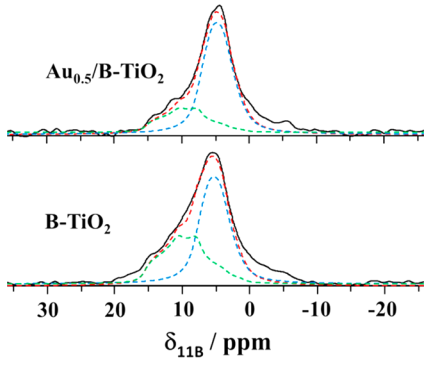

Figure 7. ^{11}B MAS NMR spectra of $Au_{0.5}$/B-TiO_2 (upper) and B-TiO_2 (bottom).

dx.doi.org/10.1021/cs5002948 | ACS Catal. 2014, 4, 1451−1457

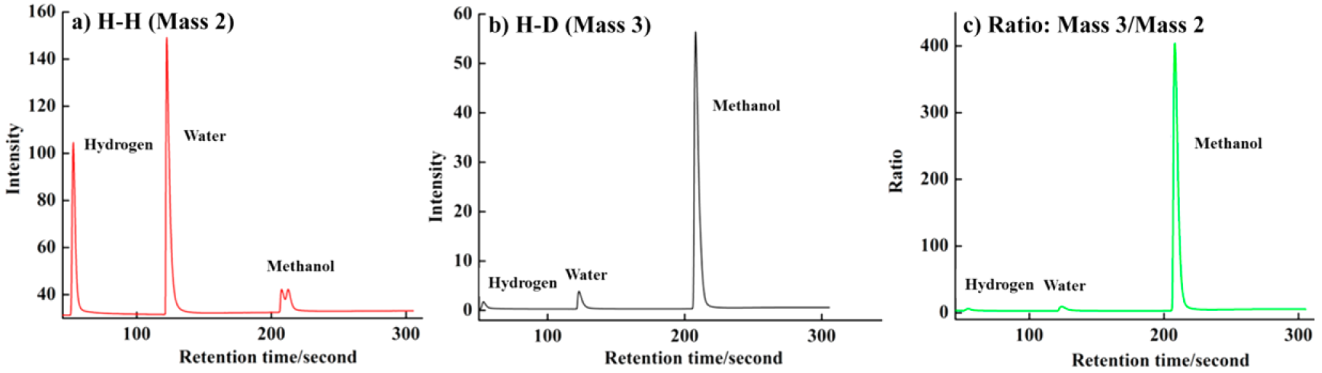

Figure 8. GC/IRMS spectra of the obtained gas when H_2O and CD_3OD were used in the suspension containing the $Au_{0.5}$/B-TiO_2 under irradiation of light (Xe lamp, 300 W): (a) H_2 (mass 2), (b) HD (mass 3), and (c) HD/H_2 (mass 3/mass 2).

On the basis of the above XPS results and earlier studies of boron species in B,Ag-codoped TiO_2,[13] the ^{11}B NMR peak of $Au_{0.5}$/B-TiO_2 can be deconvoluted into two overlapped peaks centered at 5.6 ppm and 9.6 ppm, corresponding to interstitial Ti−O−B species and surface boron oxide species (B_2O_3), respectively. For the B-TiO_2, the chemical shifts of Ti−O−B species and surface boron oxide are 6.4 and 11.1 ppm, respectively.

Estimated by the signal intensities of both species, the content of Ti−O−B species increases from 54% in B-TiO_2 to 66% in $Au_{0.5}$/B-TiO_2, indicating the embedding of gold particles into the TiO_2 framework promotes the formation of interstitial B species. That means more boron is expected to be doped into the lattice of Au/TiO_2 rather than to form a thin inactive layer of boron oxide species.[22] From the NMR results, it is apparent that $Au_{0.5}$/B-TiO_2 contains more interstitial B species than B-TiO_2. More interstitial species in vacancies or microvoids could give rise to surface or near-surface states for accommodation of Au nanoparticles. Therefore, a greater activity enhancement in $Au_{0.5}$/B-TiO_2 than that in $Au_{0.5}$/TiO_2 is understandable because of the synergistic effect between Au and B codopants.

Understanding the reaction pathway of the photocatalytic hydrogen generation from a water/methanol mixture is of great importance to design more efficient photocatalysts and reaction systems. Because of the limited studies on elucidating the mechanism of photocatalytic hydrogen generation,[23] the role of alcohols in this process needs to be better understood to devise more economical and practical applications. One simply assumed that the produced H_2 mainly comes from the alcohols derived from the phenomena that none or only a tiny amount of H_2 is produced when the alcohols are absent in the suspension.

In this work, one control experiment without adding methanol into the suspension showed that ~80 μmol/g of hydrogen was generated after 5 h of irradiation, indicating that hydrogen could be obtained from direct water splitting without a sacrificial agent. The low evolution of hydrogen and lack of oxygen generation are probably attributed to the photoreduction of the produced oxygen by the excited electrons, which reduces the hydrogen production rate.[24] As such, the introduction of the sacrificial agent, such as alcohols, is highly desirable to boost the activity. Another control experiment was undertaken under irradiation of visible light (cutoff λ > 420 nm) while the other conditions remained identical. After 5 h of irradiation, no hydrogen was evolved, and only a trace amount of CO_2 was detected (~0.55 μmol/g), as shown in Supporting Information Figure S2, indicating that the direct oxidation of methanol under visible light irradiation did not lead to hydrogen generation. Therefore, it is reasonable to postulate that the methanol acted as the hole scavenger that was oxidized to CO_2 and H_2O, and at the same time, the photogenerated electrons have the chance to reduce protons into hydrogen molecules.

To figure out the origin of generated hydrogen during the photocatalytic process, isotope ratio experiments were conducted on a GC/IRMS system, which is the most useful tool to study the natural variation in isotopic ratios. The isotopic profile of hydrogen as H−H (mass 2) and H−D (mass 3) can be compared. Figure 8 shows the GC/IRMS spectra obtained from the experiment using H_2O/CD_3OD under irradiation. It is clear that all three components—hydrogen, water, and methanol—show a mass 2 peak (H_2) in Figure 8a and a mass 3 peak (HD) in Figure 8b, indicating the H−D exchange between H_2O and CD_3OD occurred, forming HDO and CD_3OH.[25] However, CD_3OD was still dominating in the mixed components of CD_3OD and CD_3OH, as evidenced by the fact that the mass 3 peak was the dominating CD_3OD peak in the experiment using H_2O/CD_3OD. It is further confirmed by the completely different isotopic profiles obtained from the control experiment using D_2O/CH_3OH.

Figure 8c shows that the isotopic profile (mass 3/mass 2) of the produced hydrogen is much closer to the hydrogen in water compared with the hydrogen in methanol, which indicates that most of the generated hydrogen originated from water rather than methanol. If the hydrogen comes from methanol, then the number of D_2 would be greater than that of HD, followed by H_2. However, from the spectra, the number for H_2 is much larger than HD, thus ruling out the proposal that the hydrogen comes mainly from methanol. If the hydrogen gas comes from water molecules, then the number of H_2 should exceed that of HD, which agrees well with the present GC/IRMS spectra. To further verify this conclusion, a control experiment with the suspension using D_2O/CH_3OH was conducted. The corresponding GC/IRMS spectra are shown in Supporting Information Figure S3. The spectrum shows that the isotope ratio (mass 3/mass 2) of the generated hydrogen is much greater than 1 and closer to the hydrogen in water, and this further supports that the evolved hydrogen gas originates mainly from water molecules.

To elucidate the role of methanol in the photocatalytic hydrogen generation process, the intermediates/products in the aqueous suspension were analyzed at intervals by HPLC. As shown in Figure 9, prior to photoirradiation, no product was

dx.doi.org/10.1021/cs5002948 | ACS Catal. 2014, 4, 1451−1457

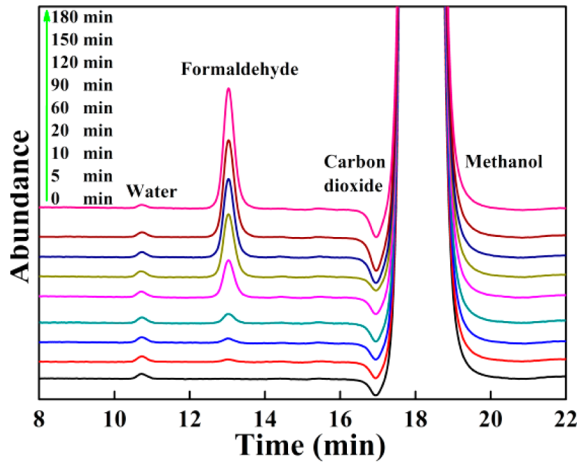

Figure 9. HPLC results of the intermediates and products at intervals from the water/methanol mixture (volume ratio = 9:1) in the suspension containing the $Au_{0.5}$/B-TiO_2 under irradiation of light (Xe lamp, 300 W).

detected except for the added water and methanol in the system. After 5 min of irradiation, a formaldehyde peak appeared. With the increase in the irradiation time, the intensity of formaldehyde grew, indicating continuous formation of formaldehyde. This finding means that Au/B-TiO_2 is capable of oxidizing methanol with protons/water as an electron acceptor under oxygen-free conditions.

On the basis of the above GC/IRMS combined with the HPLC results, a possible reaction pathway for photocatalytic hydrogen generation on Au-embedded boron-doped TiO_2 is proposed. As shown in Scheme 1, the embedded gold

Scheme 1. The Proposed Reaction Pathway of Photocatalytic Hydrogen Generation from Water/Methanol Suspension Containing Au/B-TiO_2 Catalyst

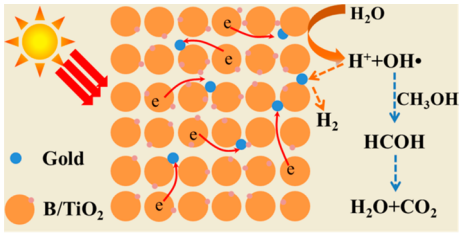

nanoparticles probably sitting in close proximity to Ti-O-B interstitial boron species act as efficient sinks for the excited electrons. Upon irradiation, the photoinduced electrons are easily transferred from the TiO_2 to the Au nanoparticles and form new traps. It, in turn, prolongs the lifetime of the charge carriers. The holes in the valence band migrate to the surface of TiO_2 and react with the adsorbed water molecules, forming the hydroxyl radicals and hydrogen ion. In the following step, the hydroxyl radicals would attack the methanol molecules and oxidize them into formaldehyde, which is further oxidized to CO_2 and water. In the meantime, the photogenerated electrons trapped on the gold nanoparticles facilitate the reduction of hydrogen ions into hydrogen molecules.

CONCLUSIONS

Gold-embedded boron-doped TiO_2 photocatalysts were successfully synthesized by a one-pot sol–gel hydrothermal method. Evidenced by XPS and ^{11}B MAS NMR, embedding of gold particles into the TiO_2 framework facilitates the formation of more interstitial boron species. Such interstitial boron species in vacancies or microvoids, in turn, give rise to surface or near-surface states for accommodation of Au nanoparticles in the B-TiO_2 framework. This unique synergistic effect for the Au/B-TiO_2 photocatalyst preferentially promotes a remarkable enhancement in hydrogen evolution from a water/methanol mixture. This study provides a new route to synthesis of highly efficient and stable TiO_2-based photocatalysts for hydrogen generation.

Furthermore, experimental evidence shows that hydrogen could be generated from reducing pure water in the absence of methanol, while the direct oxidation of methanol would not lead to the hydrogen evolution. Isotope tracer experiments reveal that most of the produced hydrogen comes from water rather than methanol. Acting as a sacrificial reagent, methanol can be oxidized to formaldehyde by protons/water in the oxygen-free conditions. This fundamental understanding is important for the rational design of a more economical and practical hydrogen production system.

ASSOCIATED CONTENT

Supporting Information

XRD, BET surface area, CO_2 evolution profile from the methanol oxidation, and GC/IRMS spectra when D_2O and CH_3OH were used. This material is available free of charge via the Internet at http://pubs.acs.org.

AUTHOR INFORMATION

Corresponding Authors

*Phone: +612-9385-7355. Fax: +612-9385-5966. E-mail: yijiao.jiang@unsw.edu.au

*Phone: +612-9385-4361. Fax: +612-9385-5966. E-mail: r.amal@unsw.edu.au

Notes

The authors declare no competing financial interests.

ACKNOWLEDGMENTS

We are grateful for facility use from UNSW Mark Wainwright Analytical Centre at UNSW Australia. Financial support by the Australian Research Council Discovery Early Career Researcher Award (DE120100329) and Australian Research Council Discovery Project (DP140102432) are gratefully acknowledged.

REFERENCES

(1) (a) Kudo, A.; Miseki, Y. *Chem. Soc. Rev.* **2009**, *38*, 253–278. (b) Iwase, A.; Teoh, W. Y.; Amal, R. *Chem. Lett.* **2011**, *40*, 108–110.

(2) (a) Choi, W.; Termin, A.; Hoffmann, M. R. *J. Phys. Chem.* **1994**, *98*, 13669–13679. (b) Teoh, W. Y.; Scott, J. A.; Amal, R. *J. Phys. Chem. Lett.* **2012**, *3*, 629–639. (c) Fujishima, A.; Rao, T. N.; Tryk, D. A. *J. Photochem. Photobiol. C* **2000**, *1*, 1–21.

(3) (a) Jiao, W.; Wang, L.; Liu, G.; Lu, G. Q.; Cheng, H.-M. *ACS Catal.* **2012**, *2*, 1854–1859. (b) Gartner, F.; Losse, S.; Boddien, A.; Pohl, M. M.; Denurra, S.; Junge, H.; Beller, M. *ChemSusChem* **2012**, *5*, 530–533. (c) Kho, Y. K.; Iwase, A.; Teoh, W. Y.; Mädler, L.; Kudo, A.; Amal, R. *J. Phys. Chem. C* **2010**, *114*, 2821–2829.

(4) Kim, J.; Monllor-Satoca, D.; Choi, W. *Energy Environ. Sci.* **2012**, *5*, 7647–7656.

(5) Primo, A.; Corma, A.; Garcia, H. *Phys. Chem. Chem. Phys.* **2011**, *13*, 886–910.

(6) Yang, J.; Wang, D.; Han, H.; Li, C. *Acc. Chem. Res.* **2013**, *46*, 1900–1909.

(7) (a) Lam, S. W.; Chiang, K.; Lim, T. M.; Amal, R.; Low, G. K. C. *Appl. Catal., B* **2007**, *72*, 363−372. (b) Wang, F.; Jiang, Y.; Wen, X.; Xia, J.; Sha, G.; Amal, R. *ChemCatChem* **2013**, *5*, 3557−3561.
(8) (a) Bian, Z. F.; Zhu, J.; Cao, F. L.; Lu, Y. F.; Li, H. X. *Chem. Commun.* **2009**, 3789−3791. (b) Li, H.; Bian, Z.; Zhu, J.; Huo, Y.; Li, H.; Lu, Y. *J. Am. Chem. Soc.* **2007**, *129*, 4538−4539.
(9) Chen, X.; Mao, S. S. *Chem. Rev.* **2007**, *107*, 2891−2959.
(10) In, S.; Orlov, A.; Berg, R.; Garcia, F.; Pedrosa-Jimenez, S.; Tikhov, M. S.; Wright, D. S.; Lambert, R. M. *J. Am. Chem. Soc.* **2007**, *129*, 13790−13791.
(11) Liu, G.; Zhao, Y. N.; Sun, C. H.; Li, F.; Lu, G. Q.; Cheng, H. M. *Angew. Chem., Int. Ed.* **2008**, *47*, 4516−4520.
(12) Feng, N.; Zheng, A.; Wang, Q.; Ren, P.; Gao, X.; Liu, S.-B.; Shen, Z.; Chen, T.; Deng, F. *J. Phys. Chem. C* **2011**, *115*, 2709−2719.
(13) Feng, N.; Wang, Q.; Zheng, A.; Zhang, Z.; Fan, J.; Liu, S.-B.; Amoureux, J.-P.; Deng, F. *J. Am. Chem. Soc.* **2013**, *135*, 1607−1616.
(14) Kim, J.; Lee, J.; Choi, W. *Chem. Comm.* **2008**, 756−758.
(15) Linic, S.; Christopher, P.; Ingram, D. B. *Nat. Mater.* **2011**, *10*, 911−921.
(16) Yonezawa, T.; Matsune, H.; Kunitake, T. *Chem. Mater.* **1998**, *11*, 33−35.
(17) Zheng, Z.; Huang, B.; Qin, X.; Zhang, X.; Dai, Y.; Whangbo, M.-H. *J. Mater. Chem.* **2011**, *21*, 9079−9087.
(18) Liu, G.; Zhao, Y.; Sun, C.; Li, F.; Lu, G. Q.; Cheng, H.-M. *Angew. Chem., Int. Ed.* **2008**, *47*, 4516−4520.
(19) (a) Su, K.; Ai, Z.; Zhang, L. *J. Phys. Chem. C* **2012**, *116*, 17118−17123. (b) In, S.; Orlov, A.; Berg, R.; García, F.; Pedrosa-Jimenez, S.; Tikhov, M. S.; Wright, D. S.; Lambert, R. M. *J. Am. Chem. Soc.* **2007**, *129*, 13790−13791.
(20) (a) Arabatzis, I. M.; Stergiopoulos, T.; Andreeva, D.; Kitova, S.; Neophytides, S. G.; Falaras, P. *J. Catal.* **2003**, *220*, 127−135. (b) Wang, X. D.; Waterhouse, G. I. N.; Mitchell, D. R. G.; Prince, K.; Caruso, R. A. *ChemCatChem* **2011**, *3*, 1763−1771.
(21) Feng, N.; Zheng, A.; Wang, Q.; Ren, P.; Gao, X.; Liu, S.-B.; Shen, Z.; Chen, T.; Deng, F. *J. Phys. Chem. C* **2011**, *115*, 2709−2719.
(22) Jung, K. Y.; Park, S. B.; Ihm, S.-K. *Appl. Catal., B* **2004**, *51*, 239−245.
(23) (a) Montini, T.; Gombac, V.; Sordelli, L.; Delgado, J. J.; Chen, X.; Adami, G.; Fornasiero, P. *ChemCatChem* **2011**, *3*, 574−577. (b) Gu, Q.; Long, J.; Fan, L.; Chen, L.; Zhao, L.; Lin, H.; Wang, X. *J. Catal.* **2013**, *303*, 141−155.
(24) Mills, A.; Porter, G. *J. Chem. Soc., Faraday Trans. 1* **1982**, *78*, 3659−3669.
(25) (a) Bureiko, S. F.; Golubev, N. S.; Denisov, G. S.; Lange, I. Y. *React. Kinet. Catal. Lett.* **1977**, *7*, 139−144. (b) Halford, J. O.; Pecherer, B. *J. Chem. Phys.* **1938**, *6*, 571−575.